Switching at Less Than 60 mV/Decade with a "Cold" Metal as the Injection Source

Fei Liu*

Institute of Microelectronics and Key Laboratory of Microelectronics Devices and Circuits (MoE), Peking University, Beijing 100871, China

(Received 18 November 2019; revised manuscript received 21 February 2020; accepted 7 May 2020; published 16 June 2020)

Power dissipation is a great challenge for the continuous scaling down and performance improvement of CMOS technology, due to the thermionic-current switching limit of conventional MOSFETs. In this paper, we show that this problem can be overcome by using a "cold" metal as the injection source of a transistor; these metals are different from conventional metals and can filter out high-energy electrons to break the "Boltzmann tyranny." It is proved that the subthreshold swing of the thermionic current of a transistor using a "cold"-metal contact can be much smaller than 60 mV/decade at room temperature. Specifically, the two-dimensional transition-metal-dichalcogenide (TMD) "cold" metals NbX_2 and TaX_2 ($X = \mathrm{S},\ \mathrm{Se},\ \mathrm{Te}$) are proposed as injection sources for FETs. Quantum transport simulations indicate that a promising switching efficiency and *on*-state current can be achieved using TMD "cold"-metal injection sources, which is beneficial for energy efficiency.

DOI: 10.1103/PhysRevApplied.13.064037

I. INTRODUCTION

Power consumption is becoming increasingly severe with improvements in the degree of integration, and is becoming an important bottleneck in the advancement of CMOS technology according to Moore's law [1,2]. High power consumption not only increase the chip temperature and failure rate, but also increases the chip design, packaging, and cooling costs. Especially with the rise in the use of various mobile electronic devices, such as smartphones, wearable devices, and the Internet of Things, the demand for a reduction in the power consumption of chips is becoming increasingly strong. Both the static and the dynamic power consumption of a chip are related to the supply voltage, and so lowering the supply voltage is an effective way to reduce the power consumption of a chip [1,2]. However, this is subject to a limit imposed by the transistor subthreshold swing (SS), which cannot be lower than 60 mV/decade at room temperature.

Steep-slope devices have attracted much attention for designing power-constrained applications using tunneling [3,4], impact ionization [5], and negative capacitance [6]. Recently, cold-source FETs (CS-FETs) have been proposed to obtain subthermionic switching by engineering the density of states (DOS) of the source to cut off the Boltzmann tail of the current [7]. Such cold sources can be realized by using the emerging Dirac materials [8,9], appropriately doped semiconductors [7,8], or a narrow-energy conduction band of dangling bonds [10]. However, these proposed cold sources require appropriate doping and heterogeneous integration. An ideal solution would be to find some kind of "cold" metal that can replace conventional metals in the contacts of transistors. Such "cold" metals would filter out high-energy electrons in the subthreshold region.

In this paper, a steep-slope device using a "cold"-metal contact is proposed. Here, a "cold" metal is applied to replace a conventional metal in a FET contact. Unlike conventional metals, "cold" metals have an energy gap around the Fermi level and work like *p*- or *n*-type doped semiconductors. Therefore, electrons in this energy region can be effectively filtered out, which results in switching at less than 60 mV/decade. With the emergence of two-dimensional (2D) materials, such metallic materials with the required properties can be found in monolayer (ML) NbX_2 and TaX_2 ($X = \mathrm{S},\ \mathrm{Se},\ \mathrm{Te}$), which can be obtained by mechanical exfoliation [11,12], chemical exfoliation [13–15], or chemical vapor deposition (CVD) [16–20]. We investigate 2D heterojunction CS-FETs using "cold"-metal contacts consisting of metallic transition-metal dichalcogenides (TMDs) as the injection source by quantum transport simulations using the nonequilibrium Green's function (NEGF) formalism. It is demonstrated that CS-FETs with a TMD "cold"-metal contact have promising device performance for energy-efficient switching and high *on*-state current. Our work reveals a design rule for future steep-slope electronic devices using "cold"-metal contacts.

*feiliu@pku.edu.cn

II. RESULTS AND DISCUSSION

A. "Cold" metals

Metals exist widely in nature and are very important substances in the semiconductor industry. In MOSFETs, metallic materials are used in contacts, gates, and interconnects. Usually, bulk metals have excellent electrical conductivity and have a continuous DOS around the Fermi level. Recently, 2D metallic materials have been investigated intensively due to their exotic properties [21]. Theoretical studies predict that the conventional Richardson's law for thermionic injection from bulk contact materials is not valid for Schottky contacts based on 2D materials, which have a different universal temperature scaling of their thermionic emission [22,23]. When the dimensionality is reduced from that of a bulk metallic TMD to the atomically thin limit, $2H$-$NbSe_2$ has been found to exhibit intriguing quantum phenomena of superconductivity and charge density waves [12,24–26]. Monolayer $2H$-NbS_2 has been synthesized epitaxially and applied as an injection source in 2D FETs using lateral and vertical NbS_2-WS_2 heterostructures [20].

Here, we first investigate the electronic properties of metallic TMDs by density-functional-theory (DFT) calculations, which are performed using the Vienna *ab initio* simulation package (VASP) [27]. The core-valence interaction is described by the projector-augmented-wave method [28,29]. The exchange-correlation functional of metallic TMDs is described by the generalized gradient approximation of Perdew, Burke, and Ernzerhof [30, 31], while band-structure calculations of semiconducting TMDs are performed using the Heyd-Scuseria-Ernzerhof HSE06 hybrid functional [32,33]. The energy cutoff for plane-wave expansion is set to 500 eV. Monkhorst-Pack k-point meshes are used for Brillouin-zone sampling with a $15 \times 15 \times 1$ grid for both structure relaxations and self-consistent calculations. The atomic structures are relaxed until the calculated residual forces are smaller than 0.01 eV/Å. A vacuum layer larger than 15 Å is used to avoid interaction of adjacent images.

One kind of TMD, $2H$-NbX_2 ($X = \mathrm{S,\ Se,\ Te}$), has a common chemical formula MX_2, with a layer of transition-metal atoms sandwiched between two layers of chalcogen atoms X, with covalent bonds. It is well known that the compounds $2H$-MoX_2 are semiconducting, with the lowest subbands contributed by the d_{z^2}, d_{xy}, and $d_{x^2-y^2}$ orbitals of the transition-metal atoms. There are five d electrons in the fourth shell, and the valence band is filled. However, Nb atoms have one fewer d electron in the outermost shell, and the Fermi level is in the valence band. The compounds $2H$-NbX_2 are metallic, and their band structures have similar shapes to those of MoX_2, as shown in Fig. 1. The single band around the Fermi level is contributed by hybridization of the d_{z^2}, d_{xy}, and $d_{x^2-y^2}$ orbitals. Similarly,

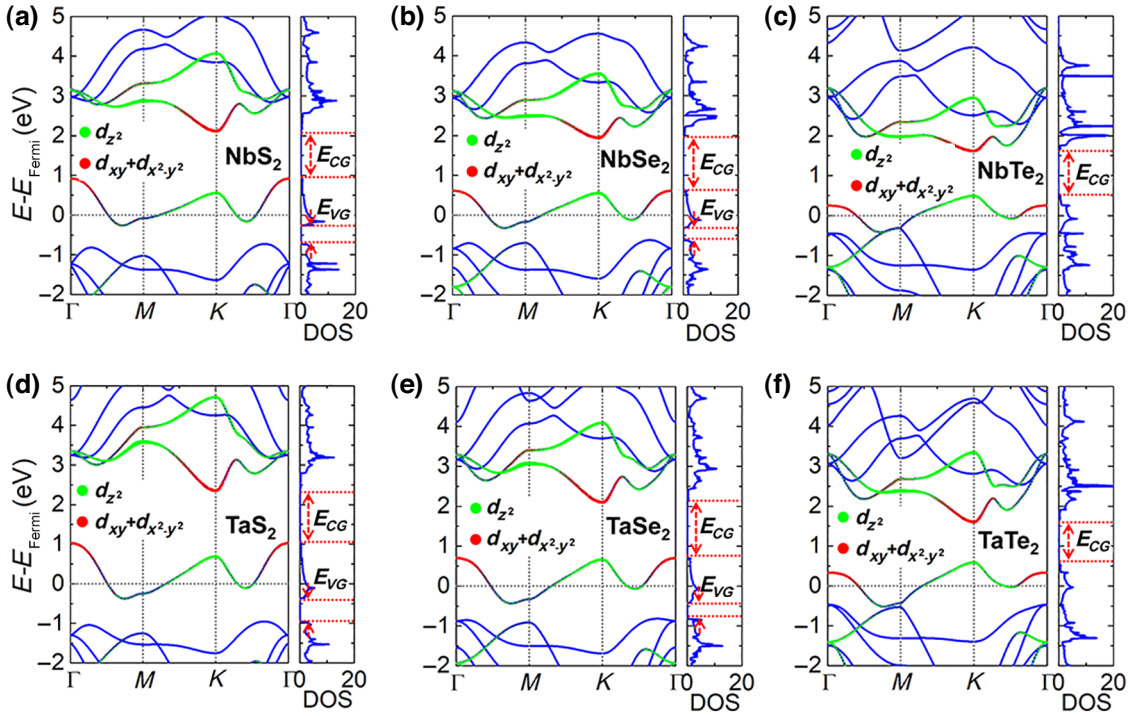

FIG. 1. Band structures of monolayer metallic MX_2 ($M = \mathrm{Nb,\ Ta}$; $X = \mathrm{S,\ Se,\ Te}$). The Fermi energy is set to zero. Differently from conventional metals, there is an energy gap in the conduction band (E_{CG}) or the valence band (E_{VG}). Therefore, electrons in the gap can be filtered out if these metallic materials are applied as the injection source of a transistor.

the compounds $2H$-TaX_2 are also metallic and have similar band structures, with the Fermi level in the topmost valence band. Unlike the case for conventional metals with a continuous density of states around the Fermi level, there is an energy gap above the chemical potential in these materials, as shown in Fig. 1. At the same time, a gap in the valence band appears below the Fermi level in NbS_2, $NbSe_2$, TaS_2, and $TaSe_2$. Therefore, these metallic materials are naturally p-type or n-type semiconductors without artificial doping. When these metallic materials are applied as the injection source of a FET, electrons with energies in the gap can be filtered out.

Next, we compare $2H$-NbX_2 and a traditional metal when used as FET contacts. Figures 2(a) and 2(d) show schematic device structures with Au and $2H$-$NbTe_2$, respectively, as injection sources. The current through the device can be calculated from the Landauer-Büttiker formula [34],

$$I_D = \frac{2q}{h}\int T(E)[f_S - f_D]\,dE, \tag{1}$$

where $T(E)$ is the transmission coefficient, and f_S and f_D are the Fermi functions of the source and drain, respectively. Figure 2(b) plots the transmission as a function of energy for a 3-nm gold film, calculated using the NEGF-DFT method implemented in Nanodcal [35]. As expected, the gold film has a continuous transport channel around the Fermi level of $E_F = 0$ eV. In contrast, Fig. 2(e) shows that there is no transport channel above 0.50 eV, due to the energy gap in the conduction band of $2H$-$NbTe_2$. The SS is given by [1,2]

$$\frac{\partial V_G}{\partial \log_{10}(I_D)}, \tag{2}$$

where V_G is the gate voltage. If the tunneling current is neglected, the SS of the thermionic current as a function of the top of the channel barrier can be calculated using the transmission of the Au contact shown in Fig. 2(c). Here, the top of the barrier is modulated by the gate voltage. It is found that the SS cannot break the switching limit of 60 mV/decade using a Au contact. Differently, $2H$-$NbTe_2$ has an energy gap in the conduction band (E_{CG}). When the top of the barrier is in this gap, the current does not change as the channel barrier is lowered, and the SS is infinitely large. In contrast, when the top of the barrier becomes lower than $E = 0.50$ eV, the current suddenly increases, and the SS is extremely small, as shown in Fig. 2(f). It is also found that the SS remains smaller than 60 mV/decade in the energy region of linearly increasing channels, which

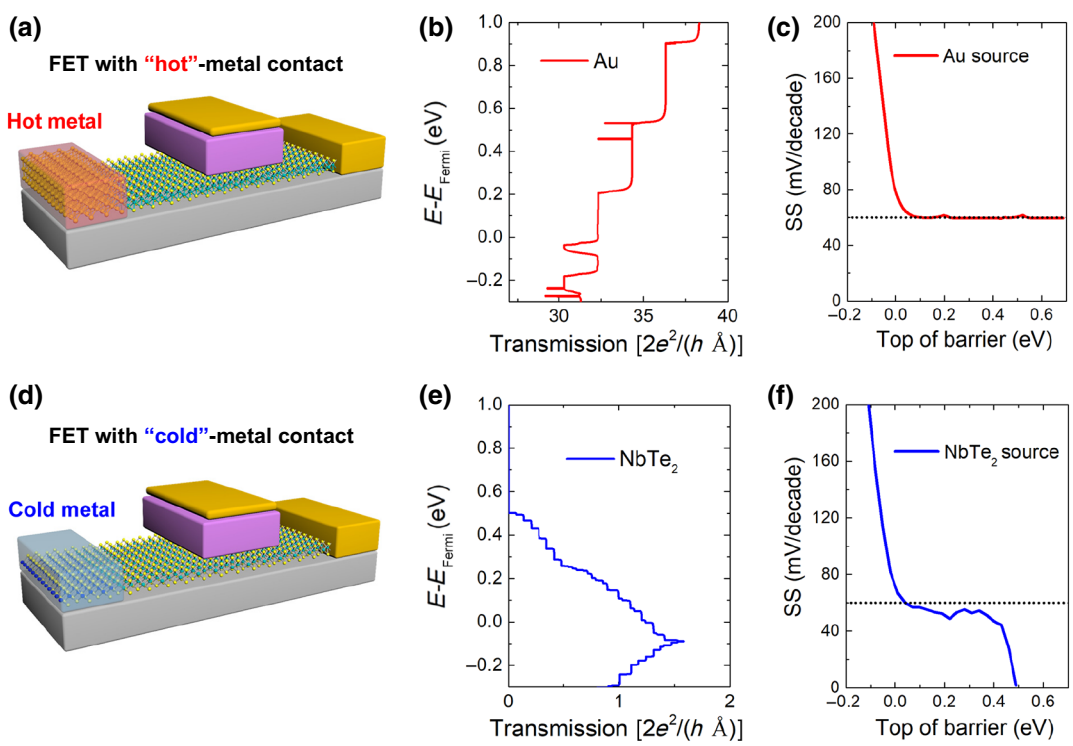

FIG. 2. Comparison between conventional "hot"-metal and "cold"-metal contacts for transistors. (a) Schematic illustration of transistor using a "hot" metal. (b) The conventional metal Au has continuous transport channels around the Fermi level. (c) The subthreshold swing of a transistor using Au is always larger than 60 mV/decade. (d) Schematic illustration of transistor using a "cold" metal. (e) The "cold" metal $NbTe_2$ has an energy region without a channel above the Fermi level. (f) The SS obtained using $NbTe_2$ as the injection source can break the thermionic limit.

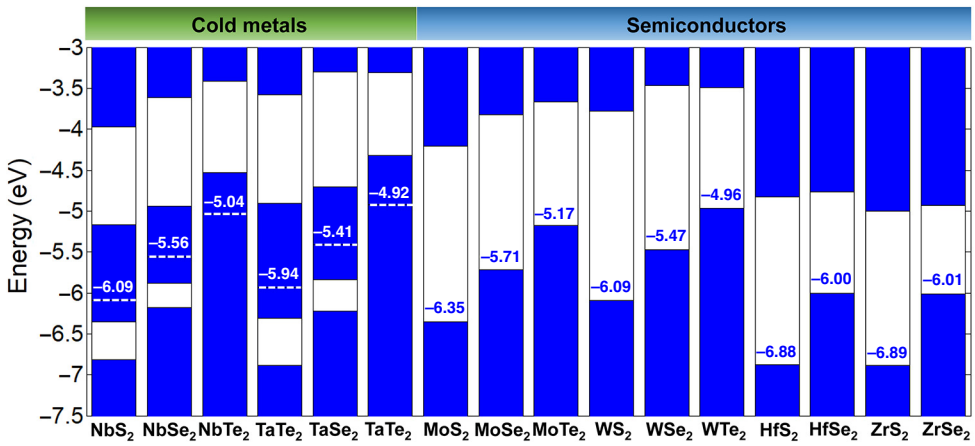

FIG. 3. Calculated band alignments for metallic and semiconducting TMDs. The dashed lines correspond to the Fermi levels of the "cold" metals. Schottky and ohmic contacts can be realized by choosing metallic and semiconducting TMDs appropriately.

is beneficial for energy-efficient switching. The physics behind this switching at less than 60 mV/decade using $2H$-$NbTe_2$ is that the high-energy electrons above the Fermi level are filtered out by the energy gap. Hence, the *off* -state current does not change when the top of the barrier is in the energy-gap region. $2H$-$NbTe_2$, when used as a FET injection source, is different from a conventional metal and works like a cold source by filtering out high-energy electrons to realize switching at less than 60 mV/decade.

The band offsets of metals and semiconductors are essential in device design. Therefore, we study the band alignments of metallic and semiconducting TMDs by first-principles calculations using VASP, as shown in Fig. 3. Here, NbX_2, TaX_2, MoX_2, and WX_2 are in the $2H$ phase, while HfX_2 and ZrX_2 are in the $1T$ phase [36]. As the atomic number of X increases (from S to Te), the Fermi level of NbX_2 increases. The Fermi levels of TaX_2 are higher than those of NbX_2 due to the much higher energy of the $5d$ orbital of the transition metal. It is found that the contacts between metallic and semiconducting TMDs are of Schottky type for the same X, such as NbS_2-MoS_2 and $NbTe_2$-$MoTe_2$ contacts. NbS_2 has the lowest Fermi level, and it is much easier to realize p-type ohmic contacts, such as NbS_2-$MoSe_2$ and NbS_2-WS_2 contacts, with it. In contrast, $TaTe_2$ has the highest chemical potential and can be applied as an n-type ohmic contact, such as in $TaTe_2$-ZrS_2 and $TaTe_2$-$ZrSe_2$ contacts.

B. Steep-slope FETs with "cold"-metal contacts

To assess the role of "cold" metals consisting of metallic TMDs as injection sources, we construct heterojunction FETs using TMDs. It has been shown that metallic NbX_2 can be exfoliated from its bulk counterpart [11,12] or synthesized by a CVD method [20]. Moreover, both lateral and vertical metal-semiconductor NbS_2-WS_2 heterostructures have been achieved [20], and these show promise as a way to construct CS-FETs using 2D-metal–semiconductor-TMD heterojunctions. We first simulate the electrical characteristics of FETs using a lateral monolayer NbS_2-WS_2 heterojunction as shown in Fig. 4(a). The monolayer NbS_2 and WS_2 are described by a three-band tight-binding model [37]. Device-performance calculations are performed by self-consistently solving the Poisson equation and Schrödinger equation within the NEGF formalism [38]. Electrons are injected from an unstrained monolayer NbS_2 contact, and 5.5% tensile strain is applied to the monolayer WS_2 due to lattice mismatch. According to the band alignment in Fig. 3, the Fermi level of NbS_2 is close to the valence-band maximum (VBM) of WS_2, and there is a p-type contact. Hence, p-type NbS_2-WS_2 CS-FETs are investigated. The source, drain, and gate lengths of the simulated FETs are 15, 15, and 10 nm, respectively. The source contains 4 nm of NbS_2 and 11 nm of p-type WS_2. The WS_2 in the source and drain is doped p-type with a doping density $p_0 = 0.02$ hole/W atom. Monolayer WS_2 has a direct-to-indirect band-gap transformation under tensile strain, and the VBM shifts from the K point to the Γ point, as shown in Fig. 4(b), which has a great impact on the device performance of NbS_2-WS_2 CS-FETs as discussed below.

Figure 4(c) shows the transfer characteristics of p-type WS_2 FETs and NbS_2-WS_2 CS-FETs at $V_D = -0.5$ V, with $I_{\text{off}} = 10^{-5}$ μA/μm at $V_G = 0.0$ V. The WS_2 FETs have ideal gate control, with a SS as small as 64 mV/decade. When NbS_2 is applied as the injection source, the switching properties can be improved significantly, as expected, and the SS is reduced to 19 mV/decade in the range -0.04 V $< V_G <$ 0.06 V. At $V_G = 0.06$ V, the top of the channel barrier is in the energy gap below the Fermi level of NbS_2, as shown in Fig. 4(d). There are no carriers from the source when the energy is lower than the energy-gap edge $E = -0.26$ eV. Therefore, the current is a direct tunneling current around the energy-gap edge. When the channel barrier is shifted to higher energy at $V_G = -0.04$ V and becomes higher than $E = -0.26$ eV, as shown in Fig. 4(e), there is both a thermionic current (42%) over the channel barrier and a tunneling current (58%). Even though the SS can be as small as 19 mV/decade, I_{on}

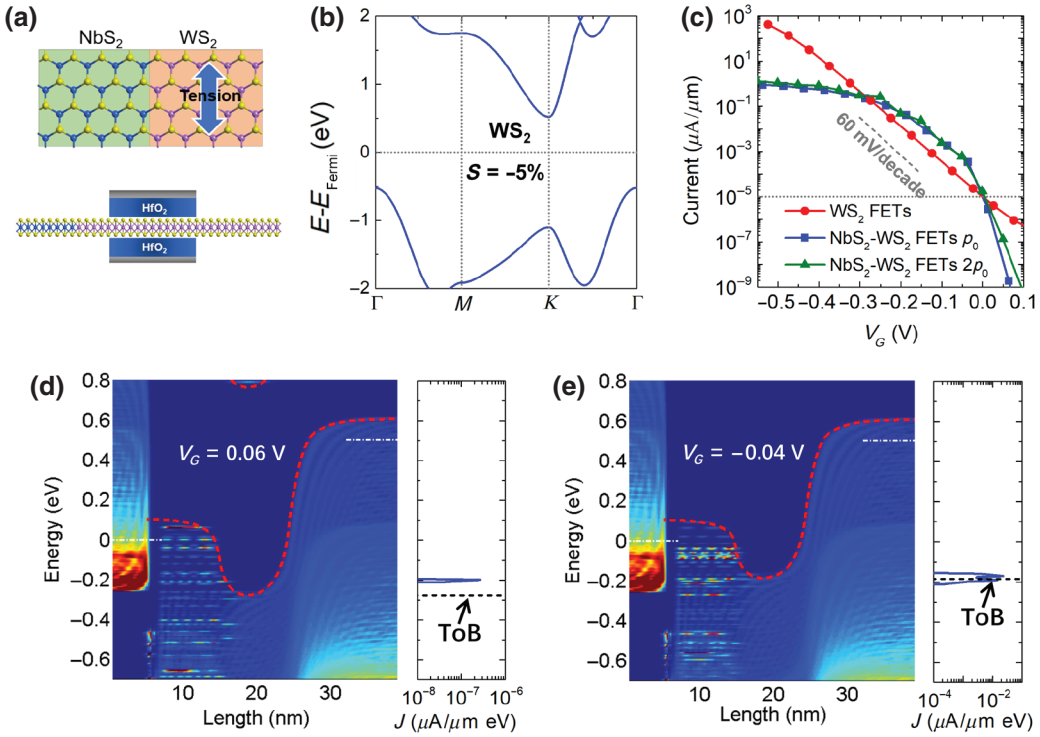

FIG. 4. Structure and performance of NbS_2-WS_2 CS-FETs. (a) Schematic device structure of heterojunction CS-FETs using NbS_2 and WS_2. (b) Band structure of monolayer WS_2 under 5.5% tensile strain. (c) I_D-V_G curves of NbS_2-WS_2 CS-FETs with monolayer WS_2 under 5.5% tensile strain at $V_D = -0.5$ V. The doping density of the WS_2 source is modulated to improve the contact resistance. (e),(f) Local density of states of NbS_2-WS_2 CS-FETs with the top of the barrier (ToB) (e) below ($V_G = 0.06$ V) and (f) above ($V_G = -0.04$ V) the edge of the energy gap of the source below the Fermi level.

of the NbS_2-WS_2 FETs is 8.4×10^{-1} μA/μm, which is much lower than that of the WS_2 FETs by two orders of magnitude. I_{on} cannot be improved effectively by increasing the doping density of the WS_2, with a reduced contact resistance, as shown in Fig. 4(c). The limitation on I_{on} when a NbS_2-WS_2 heterojunction is used can be understood from the band structures of the two materials. As shown in Fig. 1(a), the electron states around and below the Fermi level of monolayer NbS_2 are between the M point and the Γ point and between the K point and the Γ point, and are far from the Γ point, while the VBM of WS_2 under tensile strain is at the Γ point. So, there is a wave-function mismatch of the two materials in wave vector space, which determines the fundamental limitation on the *on*-state current [39].

We note that the electron states above the Fermi level in TMD "cold" metals are around the K point and that the conduction-band minima of TMD semiconductors are also at the K point. Therefore, it is possible to construct high-performance n-type FETs using TMD "cold" metals and semiconductors, due to wave-function matching in wave-vector space. An important metric for choosing an appropriate "cold" metal for an n-type FET is the energy difference between the Fermi level and the energy-gap edge in the conduction band, which is equal to 0.92, 0.62, and 0.50 eV for $2H$-NbS_2, $2H$-$NbSe_2$, and $2H$-$NbTe_2$, respectively. The energy difference cannot be too large if the electrons in the subthreshold region are to be filtered out. So, $2H$-$NbTe_2$ is chosen as the injection source, and $MoSe_2$ is used as the channel material of a CS-FET, as shown in Fig. 5(a). The two materials have a relatively small lattice mismatch. According to the band alignment, the contact between $NbTe_2$ and $MoSe_2$ is of Schottky type, and the n-type Schottky barrier is 1.21 eV, as shown in Fig. 3. Strain engineering has proved to be a promising way to tune the optical and electronic properties of 2D TMD materials [40–47]. Because of the atomic thickness of TMDs, a large strain is allowed when the material is bent, elongated, or wrinkled [48,49]. Recent experimental measurements show that 2D TMDs can withstand very large deformations of about 10% effective in-plane strain [42]. Theoretical studies also show that the elastic strain limits of TMDs can be over 14% [43,44]. So, a maximum strain of 9% is considered in our calculations. To reduce the Schottky barrier, a 5% compressive strain and a 5% tensile strain are applied to the $NbTe_2$ and $MoSe_2$, respectively. As a result, the n-type Schottky barrier is reduced to 0.09 eV.

The transfer characteristics (I_D-V_G curves) of CS-FETs and $MoSe_2$ FETs at $V_D = 0.5$ V are compared in Fig. 5(d). The metallic $NbTe_2$ has a length of 4 nm in the sources

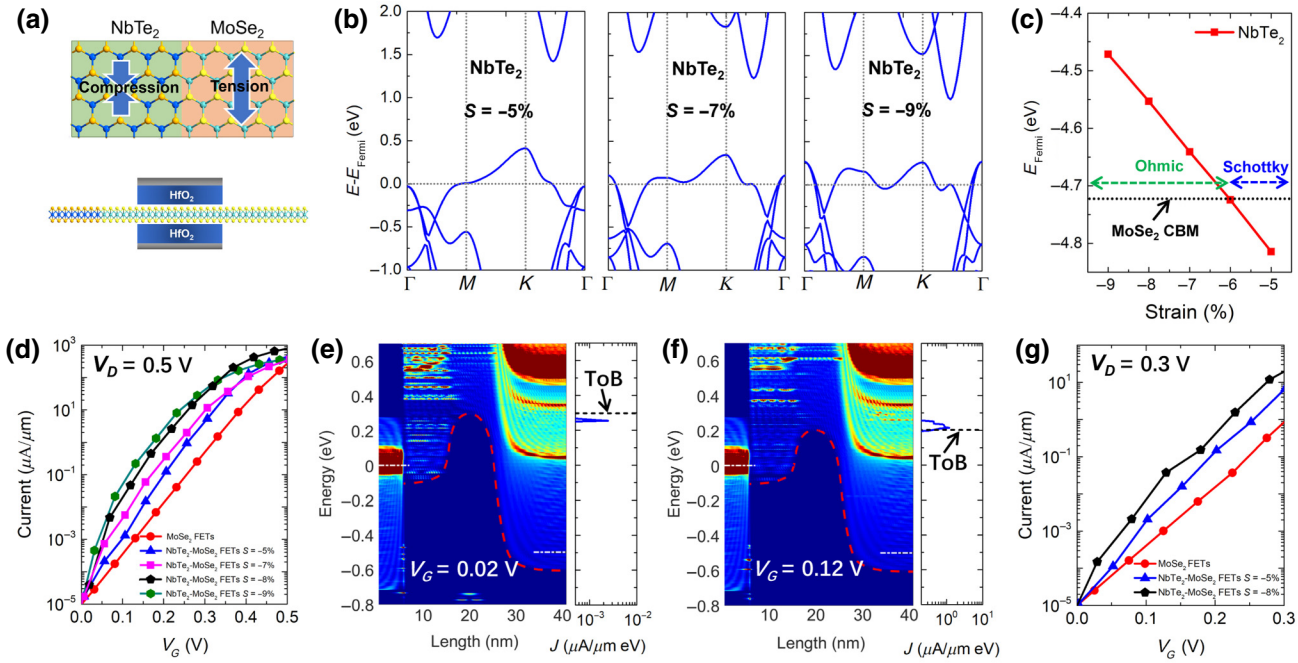

FIG. 5. Structure and performance of $NbTe_2$-$MoSe_2$ CS-FETs. (a) Schematic device structure of heterojunction CS-FETs using $NbTe_2$ and $MoSe_2$. (b) Band structure of $NbTe_2$ under compressive strain. (c) Fermi energy of $NbTe_2$ as a function of strain. Under compressive strain, the type of contact between $NbTe_2$ and $MoSe_2$ changes from a Schottky to an ohmic contact. (d) I_D-V_G curves of $NbTe_2$-$MoSe_2$ CS-FETs with $NbTe_2$ under compressive strain at $V_D = 0.5$ V. The device performance can be improved by strain. (e),(f) Local density of states of $NbTe_2$-$MoSe_2$ CS-FETs with -8% strain in the $NbTe_2$ with the ToB (e) above ($V_G = 0.02$ V) and (f) below ($V_G = 0.12$ V) the VBM of the source. (g) I_D-V_G curves of $NbTe_2$-$MoSe_2$ CS-FETs at $V_D = 0.3$ V.

of the $NbTe_2$-$MoSe_2$ CS-FETs. A three-band tight-binding model is applied to describe $2H$-$NbTe_2$ and $2H$-$MoSe_2$ [37], and the $MoSe_2$ in the source and drain regions is doped n-type. The *off* current is fixed at 10 pA/μm at $V_G = 0$ V. Compared with the $MoSe_2$ FETs, the device performance is improved in the $NbTe_2$-MoS_2 CS-FETs. The *on* current of the CS-FETs reaches 4.5×10^2 μA/μm, which is larger than the value of 3.4×10^2 μA/μm found for the $MoSe_2$ FETs. The SS of the CS-FETs is about 53 mV/decade in the range $0.0\ \text{V} < V_G < 0.1$ V, while the SS of the $MoSe_2$ FETs is around 65 mV/decade. Even though the SS of the CS-FETs breaks the switching limit, it is much larger than the theoretical prediction in Fig. 2. The reason is that the energy-gap edge above the Fermi level of $2H$-$NbTe_2$ under -5% strain is at 0.41 eV, and electrons in the deep subthreshold region are filtered out rather than those in the subthreshold region, with a current larger than 10^{-5} μA/μm. Therefore, the VBM of the $2H$-$NbTe_2$ has to be lowered in order to improve the device performance of $NbTe_2$-MoS_2 CS-FETs.

Figure 5(b) shows the band structure of $NbTe_2$ under compressive strain. As the compressive strain is increased from 5% to 9%, the energy difference between the Fermi level and the VBM decreases from 0.41 to 0.27 eV. The strain also changes the Fermi level of $NbTe_2$, as shown in Fig. 5(c). The Fermi energy increases with the compressive strain, and so the contact between $NbTe_2$ and $MoSe_2$ changes from Schottky type at $S = -5\%$ to ohmic type at $S = -9\%$. Figure 5(d) shows that the current switching is greatly improved in the $NbTe_2$-$MoSe_2$ CS-FETs as the compressive strain in the $NbTe_2$ is increased. The SS is as small as 33 and 23 mV/decade under 8% and 9% compressive strain, respectively, in the $NbTe_2$ for $0.0\ \text{V} < V_G < 0.1$ V. Figure 5(e) plots the local DOS (LDOS) along the channel at $V_G = 0.02$ V with -8% strain in the $NbTe_2$. The top of the channel barrier is above the VBM of the $NbTe_2$, and the current is composed of a 100% direct tunneling current from the source to the drain in Fig. 5(e). As the gate voltage is increased to $V_G = 0.12$ V, the ToB becomes lower than the source VBM in Fig. 5(f). As a result, 97% of the current is a thermionic current over the channel barrier. I_{on} can be as large as 7.9×10^2 μA/μm, which is larger than the value of 5.3×10^2 μA/μm in the low-power requirements of the International Technology Roadmap for Semiconductors (ITRS) 2013 [50] for $L_g = 10$ nm at $V_D = 0.75$ V. The advantages of CS-FETs become more significant as V_D is scaled to 0.3 V, as shown in Fig. 5(g). I_{on} reaches 23 μA/μm, over ten times larger than that of the $MoSe_2$ FETs, and the $I_{\text{on}}/I_{\text{off}}$ ratio is over 10^6.

We also construct $NbTe_2$-HfS_2 CS-FETs, because the Schottky-barrier height between the two materials is only

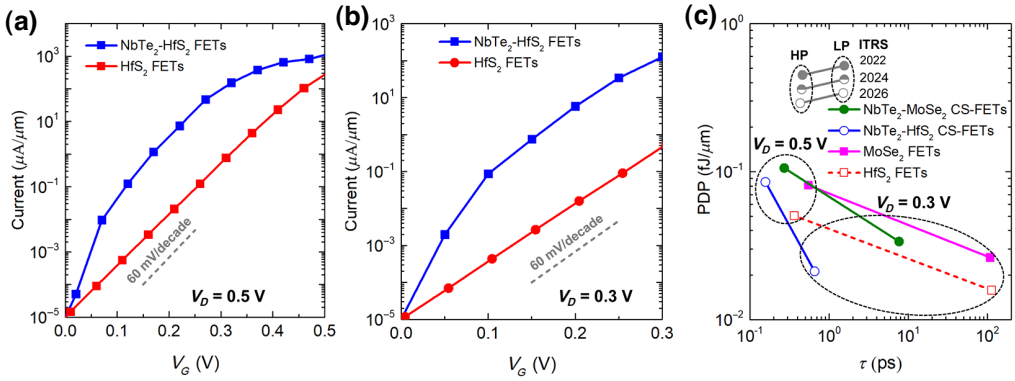

FIG. 6. Device performance of $NbTe_2$-HfS_2 CS-FETs. (a),(b) I_D-V_G curves of $NbTe_2$-HfS_2 CS-FETs and HfS_2 FETs at (a) $V_G = 0.5$ V and (b) $V_G = 0.3$ V. (c) Power-delay product and switching speed of $NbTe_2$-$MoSe_2$ CS-FETs, $NbTe_2$-HfS_2 CS-FETs, $MoSe_2$ FETs, and HfS_2 FETs compared with the requirements of ITRS 2013 [50].

0.21 eV, as shown in Fig. 3. At the same time, the lattice mismatch between the ML $NbTe_2$ and ML HfS_2 is tiny. The ML $NbTe_2$ is under −9% biaxial strain, and the ML HfS_2 is used as the channel material. Both ML $NbTe_2$ and ML HfS_2 are described by an 11-band tight-binding model [51] based on maximally localized Wannier functions [52,53]. Because of the ohmic contact, the device performance of the $NbTe_2$-HfS_2 CS-FETs is promising and much better than that of HfS_2 FETs, as shown in Figs. 6(a) and 6(b). I_{on} reaches 1.1×10^3 and 1.3×10^2 μA/μm at $V_D = 0.5$ and 0.3 V, respectively. We also investigate the switching speed and energy efficiency of $NbTe_2$-$MoSe_2$ and $NbTe_2$-HfS_2 CS-FETs, as shown in Fig. 6(c). The switching speed is measured by the intrinsic delay, defined as $\tau = (Q_{on} - Q_{off})/I_{on}$, where Q_{on} and Q_{off} are the total charges in the channel in the *on* and *off* states, respectively. The energy efficiency is measured by the power-delay product (PDP), given by $V_D(Q_{on} - Q_{off})$. It is found that the switching speeds and switching energies of the $NbTe_2$-$MoSe_2$ and $NbTe_2$-HfS_2 CS-FETs for $L_G = 10$ nm and $V_D = 0.5$ V are much better than the requirements of ITRS 2013 [50]. For example, the switching speed of the $NbTe_2$-HfS_2 CS-FETs is 2.9 and 9.9 times faster than the requirements of ITRS 2013 for high-performance (HP) and low-power (LP) applications, respectively, while the PDP is only 19% and 16% of the requirements for HP and LP applications, respectively. When the supply voltage is decreased to 0.3 V, the PDP and switching speed can be further improved, while the *on*-state current is decreased. $MoSe_2$ FETs and HfS_2 FETs also have a lower PDP, but the *on*-state currents are much smaller than those of CS-FETs, which also results in a longer intrinsic delay.

Large strains have been applied to improve device performance by modulating the band edge of the energy gap of the "cold" metal, which indicates that promising device characteristics can be achieved in CS-FETs using a "cold"-metal injection source. Such band-edge modulation by strain can also be achieved by chemical and electrostatic doping [54]. In real devices, charge-transfer doping can be induced by interaction between layered TMDs and the substrate [54]. At the same time, substrate-induced residual elastic strain results in a redistribution of the occupied hybridized electronic states between the transition-metal atoms and the chalcogens [44] and can cause charge inhomogeneities [55]. All these effects can affect the doping efficacy and change the energy-gap edge of the "cold" metal; this is similar to what we observe under different strains, as shown in Fig. 5(b). However, switching at less than 60 mV/decade is always achieved with such band-edge modification, as shown in Fig. 5(d), which shows that this steep switching is robust to these perturbations.

Finally, we discuss the possible magnetic state of $NbTe_2$, which may have a significant impact on the possibility of realizing switching at less than 60 mV/decade using such a "cold" metal. The transition metals Nb and Ta have one unpaired outermost electron, so a magnetic moment may appear. It has been shown that intrinsic NbX_2 has no magnetic moment, while NbS_2 and $NbSe_2$ structures can be magnetized under tensile strain [56]. It is predicted that NbS_2 and $NbSe_2$ under 10% tensile strain will be ferromagnetic at room temperature. Here, we apply $NbTe_2$ under compressive strain as a contact. The energy difference per unit cell between ferromagnetic and antiferromagnetic $NbTe_2$ under −9% strain is 30 mV. The Curie temperature T_C in the mean-field approximation can be estimated as $2\,\Delta E/(3k_B)$ according to the Heisenberg model [56], and is found to be 235 K for $NbTe_2$ under −9% strain. So, $NbTe_2$ under −9% strain is paramagnetic at room temperature.

III. CONCLUSION

In summary, steep-slope transistors using "cold" metals as the injection source are proposed and are investigated by quantum transport simulations. It is revealed that "cold" metals such as the 2D TMDs NbX_2 and TaX_2 can

effectively cut off the Boltzmann tail of electrons, due to the energy gap above the Fermi level. Therefore, switching at less than 60 mV/decade can be obtained by using such "cold" metals as the injection source. Comprehensive device simulations show that a steep subthreshold swing (23 mV/decade) and a high *on*-state current of over 7.9×10^2 μA/μm are achievable in both $NbTe_2$-$MoSe_2$ and $NbTe_2$-HfS_2 CS-FETs, which exhibit promising performance with respect to the requirements of ITRS 2013 for both high-performance and low-power applications. Our findings pave the way to using "cold"-metal materials to design steep-slope electronic devices, taking advantage of the rapid development of new materials.

ACKNOWLEDGMENTS

This work was supported by the National Natural Science Foundation of China (Grant No. 61974003) and the 111 Project (Grant No. B18001). We thank the high-performance-computing platform at Peking University for computational facilities.

[1] A. C. Seabaugh and Q. Zhang, Low voltage tunnel transistors for beyond CMOS logic, Proc. IEEE **98**, 2095 (2010).

[2] A. M. Ionescu and H. Riel, Tunnel field-effect transistors as energy efficient electronic switches, Nature **479**, 329 (2011).

[3] J. Appenzeller, Y. M. Lin, J. Knoch, and P. Avouris, Band-To-Band Tunneling in Carbon Nanotube Field-Effect Transistors, Phys. Rev. Lett. **93**, 196805 (2004).

[4] D. Sarkar, X. Xie, W. Liu, W. Cao, J. Kang, Y. Gong, S. Kraemer, P. M. Ajayan, and K. Banerjee, A subthermionic tunnel field-effect transistor with an atomically thin channel, Nature **526**, 91 (2015).

[5] K. Gopalakrishnan, P. B. Griffin, and J. D. Plummer, Impact ionization MOS (I-MOS)-Part I: Device and circuit simulations, IEEE Trans. Electron Devices **52**, 69 (2005).

[6] S. Salahuddin and S. Datta, Use of negative capacitance to provide voltage amplification for low power nanoscale devices, Nano Lett. **8**, 405 (2008).

[7] F. Liu, C. G. Qiu, Z. Y. Zhang, L. Peng, J. Wang, Z. Wu, and H. Guo, First principles simulation of energy efficient switching by source density of states engineering, IEEE Int. Electron Devices Meeting (IEDM) 763, (2018).

[8] F. Liu, C. Qiu, Z. Zhang, L. M. Peng, J. Wang, and H. Guo, Dirac electrons at the source: Breaking the 60-mV/decade switching limit, IEEE Trans. Electron Devices **65**, 2736 (2018).

[9] C. Qiu, F. Liu, L. Xu, B. Deng, M. Xiao, J. Si, L. Lin, Z. Zhang, J. Wang, H Guo, H. Peng, and L. M. Peng, Dirac source field-effect transistors as energy-efficient and high-performance electronic switches, Science **361**, 387 (2018).

[10] D. Logoteta, M. G. Pala, J. Choukroun, P. Dollfus, and G. Iannaccone, A steep-slope MoS_2-Nanoribbon MOSFET based on an intrinsic cold-contact effect, IEEE Electron Device Lett. **40**, 1550 (2019).

[11] K. S. Novoselov, D. Jiang, F. Schedin, T. J. Booth, V. V. Khotkevich, S. V. Morozov, and A. K. Geim, Two dimensional atomic crystals, Proc. Natl Acad. Sci. USA **102**, 10451 (2005).

[12] X. Xi, Z. Wang, W. Zhao, J .H. Park, K. T. Law, H. Berger, L. Forro, J. Shan, and K. F. Mak, Ising pairing in superconducting $NbSe_2$ atomic layers, Nat. Phys. **12**, 139 (2016).

[13] J. N. Coleman *et al.*, Two-dimensional nanosheets produced by liquid exfoliation of layered materials, Science **331**, 568 (2011).

[14] R. J. Smith, P. J. King, M. Lotya, C. Wirtz, U. Khan, S. De, A. O'Neill, G. S. Duesberg, J .C. Grunlan, G. Moriarty, J. Chen, J. Wang, A. I. Minett, V. Nicolosi, and J. N. Coleman, Large-scale exfoliation of inorganic layered compounds in aqueous surfactant solutions, Adv. Mater. **23**, 3944 (2011).

[15] J. Wu, J. Peng, Z. Yu, Y. Zhou, Y. Guo, Z. Li, Y. Lin, K. Ruan, C. Wu, and Y. Xie, Acid-assisted exfoliation toward metallic sub-nanopore TaS_2 monolayer with high volumetric capacitance, J. Am. Chem. Soc. **140**, 493 (2018).

[16] H. Wang, X. Huang, J. Lin, J. Cui, Y. Chen, C. Zhu, F. Liu, Q. Zeng, J. Zhou, P. Yu, and X. Wang, High-quality monolayer superconductor $NbSe_2$ grown by chemical vapour deposition, Nat. Commun. **8**, 394 (2017).

[17] J. Zhou, J. Lin, X. Huang, Y. Zhou, Y. Chen, J. Xia, H. Wang, Y. Xie, H. Yu, J. Lei, and D. Wu, A library of atomically thin metal chalcogenides, Nature **556**, 355 (2018).

[18] J. Shi, X. Chen, L. Zhao, Y. Gong, M. Hong, Y. Huan, Z. Zhang, P. Yang, Y. Li, Q. Zhang, Q. Zhang, L. Gu, H. Chen, J. Wang, S. Deng, N. Xu, and Y. Zhang, Chemical vapor deposition grown wafer-scale 2D tantalum diselenide with robust charge-density-wave order, Adv. Mater. **30**, 1804616 (2018).

[19] M. Hossain, J. Wu, W. Wen, H. Liu, X. Wang, and L. Xie, Chemical vapor deposition of 2D vanadium disulfide and diselenide and Raman characterization of the phase transitions, Adv. Mater. Interfaces **5**, 1800528 (2018).

[20] Y. Zhang, L. Yin, J. Chu, T. A. Shifa, J. Xia, F. Wang, Y. Wen, X. Zhan, Z. Wang, and J. He, Edge-epitaxial growth of 2D NbS_2-WS_2 lateral metal-semiconductor heterostructures, Adv. Mater. **30**, 1803665 (2018).

[21] Z. Zhang, P. Yang, M. Hong, S. Jiang, G. Zhao, J. Shi, Q. Xie, and Y. Zhang, Recent progress in the controlled synthesis of 2D metallic transition metal dichalcogenides, Nanotechnology **30**, 182002 (2019).

[22] Y. S. Ang, H. Y. Yang, and L. K. Ang, Universal Scaling Laws in Schottky Heterostructures Based on Two-Dimensional Materials, Phys. Rev. Lett. **121**, 056802 (2018).

[23] Y. S. Ang, Y. Chen, C. Tan, and L. K. Ang, Generalized High-Energy Thermionic Electron Jnjection at Graphene Interface, Phys. Rev. Appl. **12**, 014057 (2019).

[24] M. M. Ugeda, A. J. Bradley, Y. Zhang, S. Onishi, Y. Chen, W. Ruan, C. Ojeda-Aristizabal, H. Ryu, M. T. Edmonds, H. Z. Tsai, A. Riss, S. K. Mo, D. Lee, A. Zettl, Z. Hussain, Z. X. Shen, and M. F. Crommie, Characterization of collective ground states in single-layer $NbSe_2$, Nat. Phys. **12**, 92 (2016).

[25] X. X. Xi, H. Berger, L. Forro, J. Shan, and K. F. Mak, Gate Tuning of Electronic Phase Transitions in Two-Dimensional $NbSe_2$, Phys. Rev. Lett. **117**, 106801 (2016).

[26] Y. Cao *et al.*, Quality heterostructures from two-dimensional crystals unstable in air by their assembly in inert atmosphere, Nano Lett. **15**, 4914 (2015).

[27] G. Kresse and J. Furthmüller, Efficient iterative schemes for ab initio total-energy calculations using a plane-wave basis set, Phys. Rev. B **54**, 11169 (1996).

[28] P. E. Blöchl, Projector augmented-wave method, Phys. Rev. B **50**, 17953 (1994).

[29] G. Kresse and D. Joubert, From ultrasoft pseudopotentials to the projector augmented-wave method, Phys. Rev. B **59**, 1758 (1999).

[30] J. P. Perdew, K. Burke, and M. Ernzerhof, Generalized gradient approximation made simple, Phy. Rev. Lett. **77**, 3865 (1996).

[31] S. Grimme, Semiempirical GGA-type density functional constructed with a long-range dispersion correction, J. Comput. Chem. **27**, 1787 (2006).

[32] J. Heyd, G. E. Scuseria, and M. Ernzerhof, Hybrid functionals based on a screened Coulomb potential, J. Chem. Phys. **118**, 8207 (2003).

[33] J. Heyd, G. E. Scuseria, and M. Ernzerhof, Erratum: Hybrid functionals based on a screened Coulomb potential, J. Chem. Phys. **124**, 219906 (2006).

[34] S. Datta, *Quantum Transport: Atom to Transistor* (Cambridge University Press, Cambridge, UK, 2005).

[35] J. Taylor, H. Guo, and J. Wang, Ab initio modeling of quantum transport properties of molecular electronic devices, Phys. Rev. B **63**, 245407 (2001).

[36] C. Zhang, C. Gong, Y. Nie, K. N. Min, C. Liang, Y. J. Oh, H. Zhang, W. Wang, S. Hong, L. Colombo, R. M. Wallace, and K. Cho, Systematic study of electronic structure and band alignment of monolayer transition metal dichalcogenides in Van der Waals heterostructures, 2D Mater. **4**, 015026 (2017).

[37] G. Liu, W. Shan, Y. Yao, W. Yao, and D. Xiao, A three-band tight-binding model for monolayers of group-VIB transition metal dichalcogenides, Phys. Rev. B **88**, 085433 (2013).

[38] F. Liu, Y. Wang, X. Liu, J. Wang, and H. Guo, Ballistic transport in monolayer black phosphorus transistors, IEEE Trans. Electron Devices **61**, 3871 (2014).

[39] F. Liu, Y. Wang, X. Liu, J. Wang, and H. Guo, A theoretical investigation of orientation dependent transport in monolayer MoS_2 transistors at the ballistic limit, IEEE Electron Device Lett. **36**, 1091 (2015).

[40] H. Peelaers and C. G. Van de Walle, Effects of strain on band structure and effective masses in MoS_2, Phys. Rev. B **86**, 241401 (2012).

[41] P. Johari and V. B. Shenoy, Tuning the electronic properties of semiconducting transition metal dichalcogenides by applying mechanical strains, Acs Nano **6**, 5449 (2012).

[42] S. Bertolazzi, J. Brivio, and A. Kis, Stretching and breaking of ultrathin MoS_2, ACS Nano **5**, 9703 (2011).

[43] R. C. Cooper, C. Lee, C. A. Marianetti, X. Wei, J. Hone, and J. W. Kysar, Nonlinear elastic behavior of two-dimensional molybdenum disulfide, Phys. Rev. B **87**, 035423 (2013).

[44] J. Li, N. V. Medhekar, and V. B. Shenoy, Bonding charge density and ultimate strength of monolayer transition metal dichalcogenides, J. Phys. Chem. C **117**, 15842 (2013).

[45] K. He, C. Poole, K. F. Mak, and J. Shan, Experimental demonstration of continuous electronic structure tuning via strain in atomically thin MoS_2, Nano Lett. **13**, 2931 (2013).

[46] S. B. Desai, G. Seol, J. S. Kang, H. Fang, C. Battaglia, R. Kapadia, J. W. Ager, J. Guo, and A. Javey, Strain-induced indirect to direct bandgap transition in multilayer WSe_2, Nano Lett. **14**, 4592 (2014).

[47] A. P. Nayak, T. Pandey, D. Voiry, J. Liu, S. T. Moran, A. Sharma, C. Tan, C. H. Chen, L. J. Li, M. Chhowalla, and J. F. Lin, Pressure-dependent optical and vibrational properties of monolayer molybdenum disulfide, Nano Lett. **15**, 346 (2014).

[48] S. Manzeli, D. Ovchinnikov, D. Pasquier, O. V. Yazyev, and A. Kis, 2D transition metal dichalcogenides, Nat. Rev. Mater. **2**, 17033 (2017).

[49] Z. Dai, L. Liu, and Z. Zhang, Strain engineering of 2D materials: Issues and opportunities at the interface, Adv. Mater. **31**, 1805417 (2019).

[50] Process Integration, Devices, and Structures, (2013). Available: http://www.itrs.net/.

[51] S. Fang, R. K. Defo, S. N. Shirodkar, S. Lieu, G. A. Tritsaris, and E. Kaxiras, Ab initio tight-binding hamiltonian for transition metal dichalcogenides, Phys. Rev. B **92**, 205108 (2015).

[52] N. Marzari and D. Vanderbilt, Maximally localized generalized Wannier functions for composite energy bands, Phys. Rev. B **56**, 12847 (1997).

[53] A. A. Mostofi, J. R. Yates, G. Pizzi, Y.-S. Lee, I. Souza, D. Vanderbilt, and N. Marzari, An updated version of WANNIER90: A tool for obtaining maximally-localised Wannier functions, Comput. Phys. Commun. **185**, 2309 (2014).

[54] P. Luo, F. Zhuge, Q. Zhang, Y. Chen, L. Lv, Yu. Huang, H. Li, and T. Zhai, Doping engineering and functionalization of two-dimensional metal chalcogenides, Nanoscale Horiz. **4**, 26 (2019).

[55] A. Michail, N. Delikoukos, J. Parthenios, C. Galiotis, and K. Papagelis, Optical detection of strain and doping inhomogeneities in single layer MoS_2, Appl. Phys. Lett. **108**, 173102 (2016).

[56] Y. Zhou, Z. Wang, P. Yang, X. Zu, L. Yang, X. Sun, and F. Gao, Tensile strain switched ferromagnetism in layered NbS_2 and $NbSe_2$, ACS Nano **6**, 9727 (2012).